Optimization of anisotropically etched silicon surface-relief gratings for substrate-mode optical interconnects

Shun-Der Wu, Thomas K. Gaylord, Jonathan S. Maikisch, and Elias N. Glytsis

The optimum profiles of right-angle-face anisotropically etched silicon surface-relief gratings illuminated at normal incidence for substrate-mode optical interconnects are determined for TE, TM, and random linear (RL) polarizations. A simulated annealing algorithm in conjunction with the rigorous coupled-wave analysis is used. The optimum diffraction efficiencies of the −1 forward-diffracted order are 37.3%, 67.1%, and 51.2% for TE-, TM-, and RL-polarization-optimized profiles, respectively. Also, the sensitivities to grating thickness, slant angle, and incident angle of the optimized profiles are presented.

OCIS codes: 050.0050, 050.1950, 230.1950, 040.6040.

1. Introduction

To realize optical interconnects for chip-to-chip and board-to-chip interconnections for future photonic integrated circuits, efficient optical coupling between a light source and a guiding medium (such as a substrate or a waveguide) is needed. A common approach for providing efficient optical coupling is to use grating couplers. For example, volume gratings (VGs) have been extensively investigated for both substrate-mode optical interconnects[1–4] and guided-wave optical interconnects.[5–8] The advantages of VGs include high preferential-order coupling (>98%), a simple design rule based on the Bragg condition, and no need for chemical and etching steps.[5] However, one drawback of VGs is that they require large grating thicknesses ($\sim 25\lambda_0$, where λ_0 is the free-space wavelength) to maximize the diffraction efficiency since the refractive-index modulation of VGs is typically small ($\Delta n \lesssim 0.02$). In addition, VGs are fabricated by interferometric recording, a step that is not typically used in standard microelectronics processing. Furthermore, a step for laminating VGs onto substrates (or waveguides) may be required.

In contrast to VGs, surface-relief gratings (SRGs) based on silicon (Si) are alternatives for providing optical coupling.[9–11] The Si SRGs can be potentially integrated with silicon-on-insulator waveguides and complementary metal oxide semiconductor (CMOS) ICs to provide high-density opto-electronic circuits with complex functionality. Applying the conventional anisotropic wet etching of (100) oriented crystalline Si by tetramethyl ammonium hydroxide (TMAH) or potassium hydroxide (KOH), the Si SRGs composed of V grooves with facet angles of $\phi = \tan^{-1}\sqrt{2} = 54.736°$ and controlled depths, as shown in Fig. 1(a), can be precisely fabricated.[12–14] However, the maximum diffraction efficiencies of the ±1 forward-diffracted orders of the V-groove Si SRGs, which are designed to provide 45 deg diffracted angles with normally incident 1.55 μm wavelength plane waves for substrate-mode optical interconnects [as shown in Fig. 1(a)], are identical and are limited to 16.00%, 37.51%, and 24.30% for TE polarization, TM polarization, and random linear (RL) polarization (i.e., equal components of both TE polarization and TM polarization) respectively.

To attempt to improve the diffraction efficiency of the V-groove Si SRG, the profile of right-angle-face slanted Si SRG illuminated at normal incidence for substrate-mode optical interconnects needs to be investigated. As shown in Fig. 1(b), the right-angle-face

S.-D. Wu (gte782q@gmail.com), T. K. Gaylord, and J. S. Maikisch are with the School of Electrical and Computer Engineering, Microelectronics Research Center, Georgia Institute of Technology, Atlanta, Georgia 30332. E. N. Glytsis is with the School of Electrical and Computer Engineering, the National Technical University of Athens, Iroon Polytechniou 9, Athens 157 73, Greece.

Received 31 March 2005; revised 2 June 2005; accepted 2 June 2005.

0003-6935/06/010015-07$15.00/0

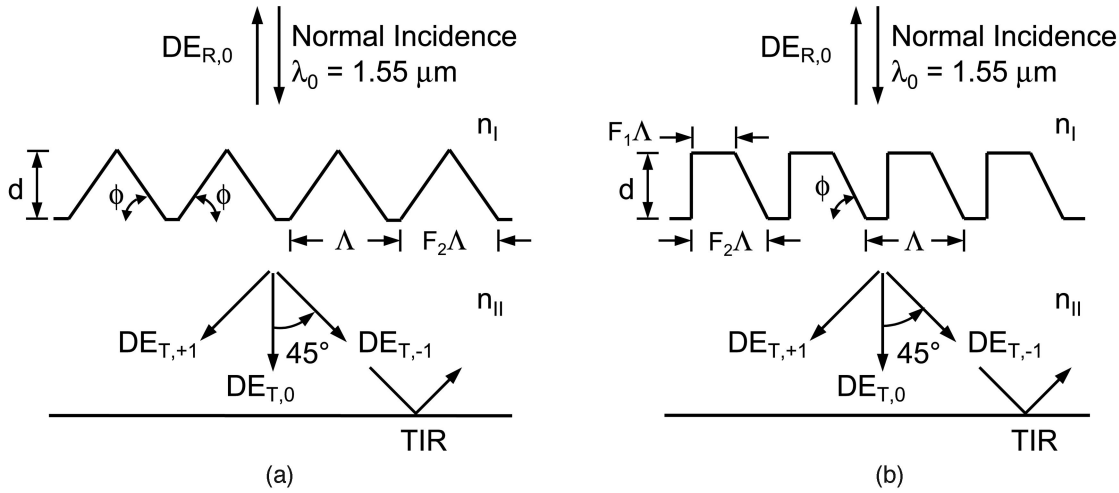

Fig. 1. Configurations of substrate-mode optical interconnects realized by (a) a V-groove Si SRG and (b) a right-angle-face slanted Si SRG illuminated by a normally incident plane wave with free-space wavelength $\lambda_0 = 1.55$ μm. The refractive indices of the incident region and Si are taken to be $n_I = 1.0$ (e.g., air) and $n_{II} = 3.475$. The Si SRGs are characterized by grating period Λ (designed to be Λ = 0.6308 μm to provide the 45 deg forward-diffracted angle of the −1 propagation order), grating thickness d, top filling factor F_1, bottom filling factor F_2, and slant angle ϕ (taken to be ϕ = 54.736° due to anisotropic etching).

slanted Si SRG can be characterized by the grating period Λ, the grating thickness d, the top filling factor F_1, the bottom filling factor F_2, and the slant angle ϕ. In order to fabricate a right-angle-face slanted Si SRG, the optical-quality surfaces produced by TMAH etching are utilized.[15] First, a layer of silicon oxide (SiO_2) is grown on Si by plasma-enhanced chemical vapor deposition, and a photoresist is spun onto the oxide. Open windows on SiO_2 for developing the right-angle-faces of a Si SRG are defined by photolithographic patterning of the photoresist followed by wet etching of SiO_2 by a buffered oxide etch (BOE) solution and removal of the photoresist. Then, utilizing an inductively coupled plasma etching followed by removal of the oxide by a BOE produces vertical grooves on the Si. The next step is to sputter a layer of gold on the Si. Similarly, applying a photolithography process and etching the gold with a $3HCl:1HNO_3$ solution defines open windows in the gold for development of slanted faces on the vertical-groove Si. Finally, a right-angle-face slanted Si SRG is produced by use of TMAH for anisotropic wet etching of the Si. This is followed by removal of the gold layer that was used to protect the vertical faces.

Although both the grating period Λ and the slant angle ϕ of a right-angle-face slanted SRG can be determined by the grating equation for a given diffracted angle and can be precisely controlled by anisotropic etching (resulting in ϕ = 54.736°), the other three parameters, d, F_1, and F_2 are not specified and have to be simultaneously optimized to obtain the maximum diffraction efficiency for substrate-mode optical interconnects. In this paper the optimized profiles of right-angle-face anisotropically etched Si SRGs for TE polarization, TM polarization, and RL polarization for substrate-mode optical interconnects are determined by use of the simulated annealing (SA) algorithm[16,17] in conjunction with a rigorous coupled-wave analysis (RCWA).[18] Furthermore, the sensitivities of these optimized profiles of right-angle-face slanted Si SRGs for TE and TM polarizations are presented.

2. Optimization of Silicon Surface-Relief Gratings

A. Simulated Annealing Optimization

The iterative method utilized in this paper for the optimization of Si SRGs is a union of the SA algorithm[16,17] and the RCWA.[18] The reasons for adopting SA as the optimization algorithm are that the SA algorithm finds the global minimum of an objective function, and the final solution is insensitive to initial values. The algorithm starts from arbitrary initial values (i.e., an initial grating profile) and, based on a step vector, performs a cycle of random moves for each grating parameter in turn to create a new grating profile. It then calculates the values of objective function f from the diffraction efficiencies determined by the use of RCWA. The number of the cycles of random moves is suggested[17] to be $N_s = 20$. Downhill moves (i.e., the change in the objective function is $\Delta f < 0$) are always accepted. On the other hand, uphill moves (i.e., the change in the objective function is $\Delta f \geq 0$) are accepted with a specified probability. The acceptance probability is given by the Boltzmann distribution $\exp(-\Delta f/T)$, where T is the normalized temperature. Here the starting normalized temperature used in the SA algorithm is $T_0 = 1.0$. With this value, a sequence of grating profiles is generated based on random changes in the grating parameters in conjunction with the acceptance probability from the Boltzmann distribution. During this phase, the step vector is increased every N_s cycles of random moves if the ratio of the number of accepted grating profiles to the number of rejected grating profiles is

Table 1. Optimization of Right-Angle-Face Slanted Si SRGs

Optimized Parameters	TE Polarization	TM Polarization	RL Polarization
d_{opt} (μm)	0.6910	0.5068	0.8410
$F_{1,\text{opt}}$	0.0000	0.3967	0.0004
$F_{2,\text{opt}}$	0.7746	0.9649	0.9432
$\text{DE}_{T,-1,\text{opt}}$ (%)	37.2891	67.0958	51.1882

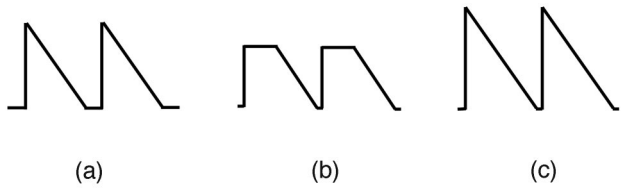

Fig. 2. Optimized profiles of right-angle-face slanted Si SRGs for (a) TE polarization, (b) TM polarization, (c) RL polarization.

greater than unity. Likewise, the step vector is decreased if this ratio is less than unity. The optimum one of all the accepted grating profiles is recorded. As the average value of f for the sequence of grating profiles reaches a stable value (i.e., reaches a state of thermal equilibrium), the normalized temperature T is decreased by a reduction coefficient[17] $r_T = 0.85$, and a new sequence of grating profiles is generated based on the previous optimum grating profile until thermal equilibrium is reached again. The process continues and is stopped when the normalized temperature is sufficiently low such that no more useful improvement is obtained. The stopping criterion used here is described in Ref. 17.

B. Optimization Results

As shown in Fig. 1(b), the substrate-mode optical interconnect is realized by a right-angle-face slanted Si SRG with a refractive index of $n_{II} = 3.475$ illuminated by a normally incident plane wave from an incident region with a refractive index of $n_I = 1.0$ (e.g., air). The free-space wavelength is $\lambda_0 = 1.55$ μm. The grating period is designed to be $\Lambda = 0.6308$ μm to provide a 45 deg forward-diffracted angle of the -1 propagation order to achieve multiple total internal reflections (TIRs) within the Si substrate, and the slant angle is taken to be $\phi = 54.736°$ due to the anisotropic etching of Si. TE polarization, TM polarization, and RL polarization of the incident plane wave are investigated. The initial values of the grating thickness and the top filling factor are set as $d = 0.5$ μm and $F_1 = 0.25$, respectively, for the SA algorithm. It is also noted that the bottom filling factor F_2 is dependent on d and F_1. Since the purpose of this research is to find the global maximum of the diffraction efficiency of the -1 forward-diffracted order, $\text{DE}_{T,-1}$, that is a function of d, F_1, and F_2 for substrate-mode optical interconnects, the objective function that will be globally minimized is defined as $f = 1/\text{DE}_{T,-1}$. To apply the RCWA to calculate the diffraction efficiencies of a right-angle-face slanted Si SRG, the SRG is decomposed into N_g rectangular subgratings. The number of N_g is selected such that the thickness of each subgrating is less than $\lambda_0/60$. Furthermore, the number of diffracted orders retained in the RCWA is nine.

Table 1 summarizes the resulting optimized parameters of right-angle-face slanted Si SRGs for TE, TM, and RL polarizations. As shown in Table 1, the optimum diffraction efficiency of TE polarization is $\text{DE}^{\text{TE}}_{T,-1,\text{opt}} = 37.29\%$, which is much smaller than the efficiency of TM polarization $\text{DE}^{\text{TM}}_{T,-1,\text{opt}} = 67.10\%$. One reason for the 29.81% higher diffraction efficiency for TM polarization (with respect to TE polarization) is that TM polarization possesses the advantage of high transmission due to the Brewster angle that is 73.946° for the air–Si planar interface. For normal incidence upon the right-angle-face slanted Si SRG, the incident angle upon slanted face is 54.736°, and the planar interface transmission for TM polarization is 87.94%, which is 38.07% more than that for TE polarization (49.87%). Apparently because of the effect of the Brewster angle, TM polarization has better performance than TE polarization. Furthermore, the optimum diffraction efficiency of RL polarization is $\text{DE}^{\text{RL}}_{T,-1,\text{opt}} = 51.19\%$ and is between the TE-optimized efficiency and the TM-optimized efficiency.

Figure 2 shows the final profiles for the TE-optimized, the TM-optimized, and the RL-optimized profiles of right-angle-face slanted Si SRGs. The optimized parameters are listed in Table 1. As shown in Fig. 2, the TE-optimized profile has a pointed top and a flat bottom. In contrast, the TM-optimized profile has a flat top and a pointed bottom. However, the RL-optimized profile has both a pointed top (like that of the TE-optimized profile) and a pointed bottom (like that of the TM-optimized profile). This set of optimized profiles is interesting and not particularly intuitive. The efficiency of the RL-optimized profile is between that of the TE-optimized profile and that of the TM-optimized profile. The performances of the TE-optimized, the TM-optimized, and the RL-optimized profiles are summarized in Table 2. As shown in Table 2, for all optimized profiles, the diffraction efficiencies for TM polarization are much higher than those for TE polarization, and the diffraction efficiencies for RL polarization are between those for TE polarization and those for TM polarization.

Table 2. Performance of Optimized Right-Angle-Face Slanted Si SRGs

Optimized Profiles	TE Polarization $\text{DE}^{\text{TE}}_{T,-1}$ (%)	TM Polarization $\text{DE}^{\text{TM}}_{T,-1}$ (%)	RL Polarization $DE^{\text{RL}}_{T,-1}$ (%)
TE	37.2891	61.4251	49.3571
TM	21.9396	67.0958	44.5177
RL	36.8003	65.5762	51.1882

3. Sensitivities of Optimized Silicon Surface-Relief Gratings

Manufacturing variations will result in deviations of the groove depth from the optimized value and of the

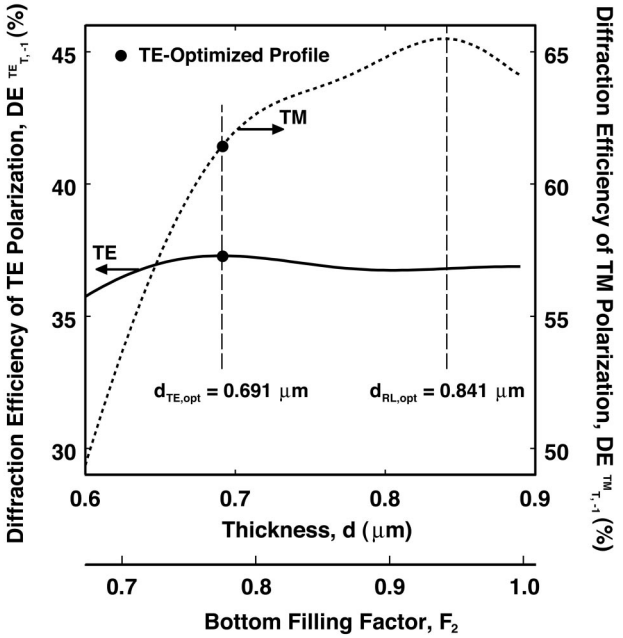

Fig. 3. Diffraction efficiencies of both TE polarization and TM polarization at normal incidence as a function of d and the corresponding F_2 based on the TE-optimized profile (i.e., $F_1 = 0.0000$ and $\phi = 54.736°$ are constants).

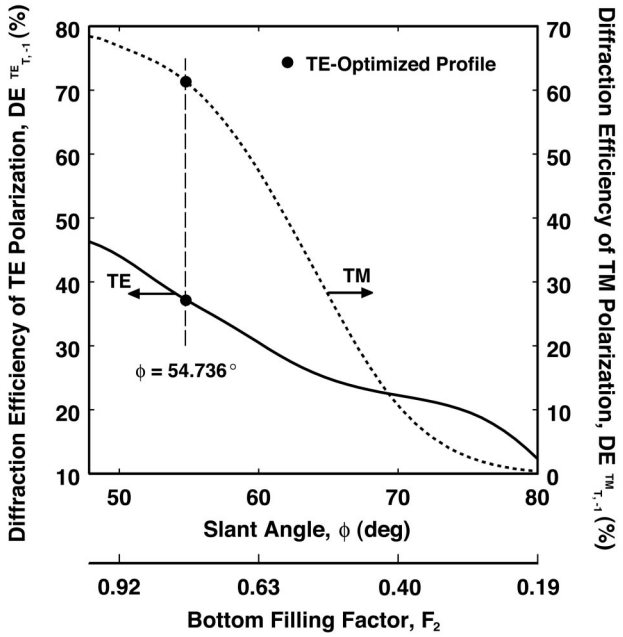

Fig. 4. Diffraction efficiencies of both TE polarization and TM polarization at normal incidence as a function of ϕ and the corresponding F_2 based on the TE-optimized profile (i.e., $d = 0.6910$ μm and $F_1 = 0.0000$ are constants).

slant angle from $\phi = 54.736°$. Therefore, the sensitivities of optimized right-angle-face slanted Si SRGs are important for practical applications. In this paper the sensitivities of the groove depth, the slant angle, as well as the incident angle for the TE-optimized profile and the TM-optimized profile of right-angle-face slanted Si SRGs are presented.

A. TE-Optimized Profile

Figure 3 shows the diffraction efficiencies of the -1 forward-diffracted order for both TE polarization $DE^{TE}_{T,-1}$ and TM polarization $DE^{TM}_{T,-1}$ at normal incidence as a function of grating thickness d and corresponding bottom filling factor F_2 based on the TE-optimized profile. As shown in Fig. 3, $DE^{TE}_{T,-1}$ decreases as d deviates from the optimum value of $d_{TE,opt} = 0.691$ μm for TE polarization. However, for TM polarization, $DE^{TM}_{T,-1}$ increases as d increases, and thus F_2 increases and reaches a local maximum $DE^{TM}_{T,-1} = 65.49\%$ (close to the TM performance of the RL-optimized profile with $DE^{TM}_{T,-1} = 65.58\%$ listed in Table 2) at $d = d_{RL,opt} = 0.841$ μm. This result is expected since the RL-optimized profile has its top filling factor like that of the TE-optimized profile. Thus, if the grating thickness increases in the TE-optimized profile, the TE-optimized profile closely approaches the RL-optimized profile.

Figure 4 shows the diffraction efficiencies of both TE polarization $DE^{TE}_{T,-1}$ and TM polarization $DE^{TM}_{T,-1}$ at normal incidence as a function of slant angle ϕ and the corresponding bottom filling factor F_2 based on the TE-optimized profile. As shown in Fig. 4, both $DE^{TE}_{T,-1}$ and $DE^{TM}_{T,-1}$ increase as ϕ decreases from the angle of anisotropic etching ($\phi = 54.736°$). On the other hand, both $DE^{TE}_{T,-1}$ and $DE^{TM}_{T,-1}$ decrease as ϕ increases from $\phi = 54.736°$. In other words, the diffraction efficiencies for both TE and TM polarizations increase (or decrease) as the incidence moves toward (or moves away from) the normal of the slanted face.

Figures 5 and 6 show the diffraction efficiencies of the -1 forward-diffracted order $DE_{T,-1}$, the 0th forward-diffracted order $DE_{T,0}$, the $+1$st forward-

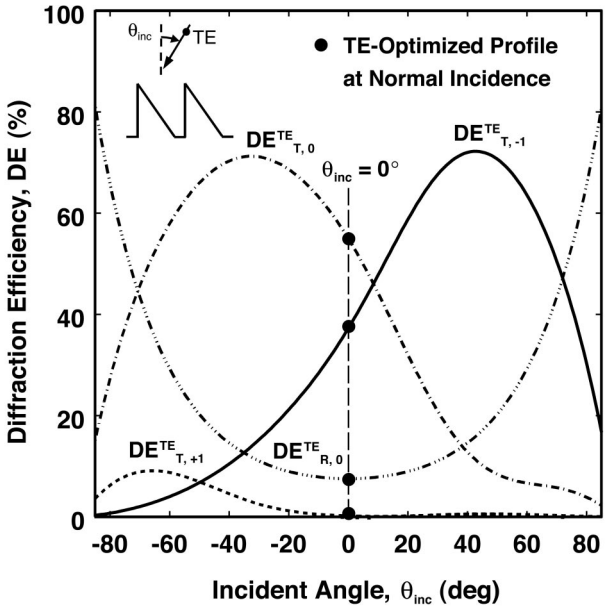

Fig. 5. Diffraction efficiencies as a function of incident angle θ_{inc} for the TE-optimized profile with a TE-polarized incidence.

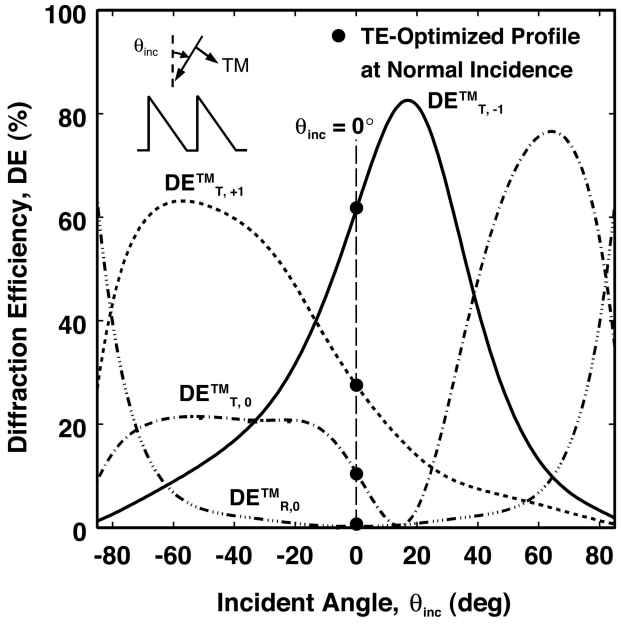

Fig. 6. Diffraction efficiencies as a function of incident angle θ_{inc} for the TE-optimized profile with a TM-polarized incidence.

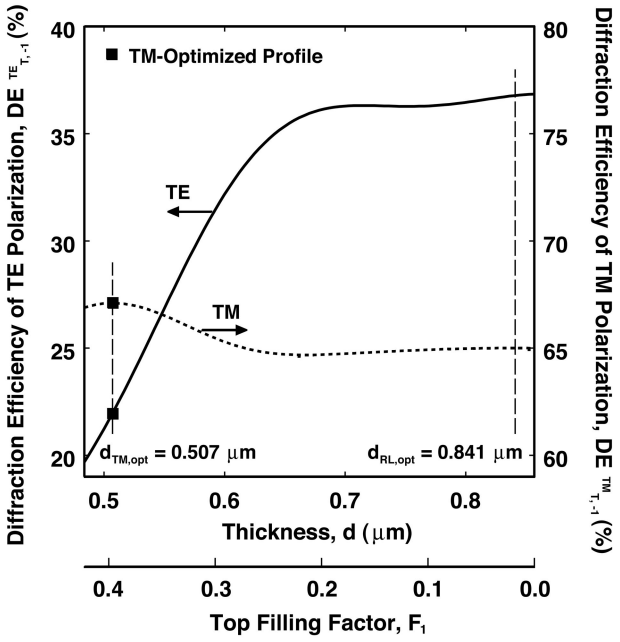

Fig. 7. Diffraction efficiencies of both TE polarization and TM polarization at normal incidence as a function of d and the corresponding F_1 based on the TM-optimized profile (i.e., $F_2 = 0.9649$ and $\phi = 54.736°$ are constants).

diffracted order $DE_{T,+1}$, and the 0th backward-diffracted order $DE_{R,0}$ as a function of the incident angle θ_{inc} for the TE-optimized profile for both TE and TM polarizations, respectively. The positive values of θ_{inc} are defined in a clockwise direction. As shown in Fig. 5, $DE^{TE}_{T,0} > DE^{TE}_{T,-1} > DE^{TE}_{T,+1}$ for TE polarization at normal incidence. In contrast, $DE^{TM}_{T,-1} > DE^{TM}_{T,+1} > DE^{TM}_{T,0}$ for TM polarization at normal incidence (shown in Fig. 6). In addition, for TE polarization, $DE^{TE}_{T,-1}$ increases as θ_{inc} increases and reaches the maximum diffraction efficiency of $DE^{TE}_{T,-1} = 72.24\%$ at $\theta_{inc} = 42.72°$ (shown in Fig. 5). Similarly, for TM polarization, $DE^{TM}_{T,-1}$ increases as θ_{inc} increases and reaches the maximum diffraction efficiency of $DE^{TM}_{T,-1} = 82.64\%$ at $\theta_{inc} = 17.61°$ (shown in Fig. 6). In other words, the diffraction efficiencies of the -1 forward-diffracted order for both TE and TM polarizations increases as the incidence moves toward the normal of the slanted face, a result that is consistent with the sensitivity analysis of the slant angle (Fig. 4). Furthermore, the diffraction efficiency of the $+1$ forward-diffracted order of TM polarization (the curve of $DE^{TM}_{T,+1}$ in Fig. 6) is much larger than that of TE polarization (the curve of $DE^{TE}_{T,+1}$ in Fig. 5). Finally, because of the effect of the Brewster angle, the diffraction efficiency of the 0th backward-diffracted order of TM polarization (the curve of $DE^{TM}_{R,0}$ in Fig. 6) is smaller than that of TE polarization (the curve of $DE^{TE}_{R,0}$ in Fig. 5).

B. TM-Optimized Profile

Figure 7 shows the diffraction efficiencies of both TE polarization $DE^{TE}_{T,-1}$ and TM polarization $DE^{TM}_{T,-1}$ at normal incidence as a function of grating thickness d and the corresponding top filling factor F_1 based on the TM-optimized profile. As shown in Fig. 7, $DE^{TM}_{T,-1}$ decreases as d deviates from the optimum value of $d_{TM,opt} = 0.507\ \mu m$ for TM polarization. On the other hand, as d increases (and thus F_1 decreases), $DE^{TE}_{T,-1}$ increases for TE polarization. As d increases to $d_{RL,opt} = 0.841\ \mu m$, the diffraction efficiency is $DE^{TE}_{T,-1} = 36.78\%$ close to the TE performance of the RL-optimized profile with $DE^{TE}_{T,-1} = 36.80\%$ (Table 2) because the RL-optimized profile has its bottom filling factor like that of TM-optimized profile. As a result, if the grating thickness increases in the TM-optimized profile, the TM-optimized profile closely approaches the RL-optimized profile. This behavior of the TE performance of the TM-optimized profile is similar to that of the TM performance of the TE-optimized profile (Subsection 3.A).

Figure 8 shows the diffraction efficiencies of both TE polarization $DE^{TE}_{T,-1}$ and TM polarization $DE^{TM}_{T,-1}$ at normal incidence as a function of slant angle ϕ and the corresponding F_1 based on the TM-optimized profile. As shown in Fig. 8, for TE polarization, $DE^{TE}_{T,-1}$ increases (or decreases) as ϕ decreases (or increases) from $\phi = 54.736°$, which is consistent with the TE performance of the TE-optimized profile (Fig. 4). However, for TM polarization, $DE^{TM}_{T,-1}$ decreases as ϕ increases, but remains almost constant as ϕ decreases. In general, the diffraction efficiencies for both TE and TM polarizations increase (or decrease) as the incidence moves toward (or moves away from) the normal of the slanted face in agreement with the results of the TE-optimized profile.

Figures 9 and 10 show the diffraction efficiencies of $DE_{T,-1}$, $DE_{T,0}$, $DE_{T,+1}$, and $DE_{R,0}$ as a function of incident angle θ_{inc} for the TM-optimized profile for both

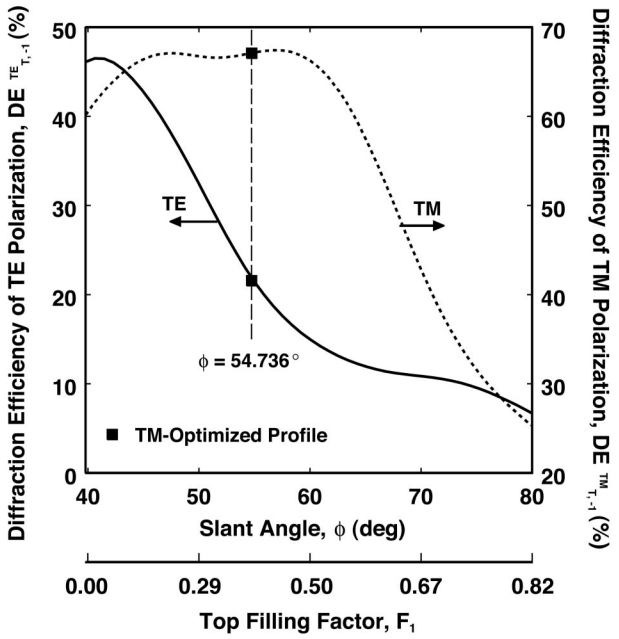

Fig. 8. Diffraction efficiencies of both TE polarization and TM polarization at normal incidence as a function of ϕ and the corresponding F_1 based on the TM-optimized profile (i.e., $d = 0.5068$ μm and $F_2 = 0.9649$ are constants).

TE and TM polarizations, respectively. Similar to the cases of the TE-optimized profile (shown in Figs. 5 and 6), for the TM-optimized profile at normal incidence, $DE^{TE}_{T,0} > DE^{TE}_{T,-1} > DE^{TE}_{T,+1}$ for TE polarization (Fig. 9), and $DE^{TM}_{T,-1} > DE^{TM}_{T,+1} > DE^{TM}_{T,0}$ for TM polarization (Fig. 10). The diffraction efficiencies of $DE^{TE}_{T,-1}$ increase as θ_{inc} increases and reach the maximum values of $DE^{TE}_{T,-1} = 51.35\%$ at $\theta_{inc} = 35.16°$ and

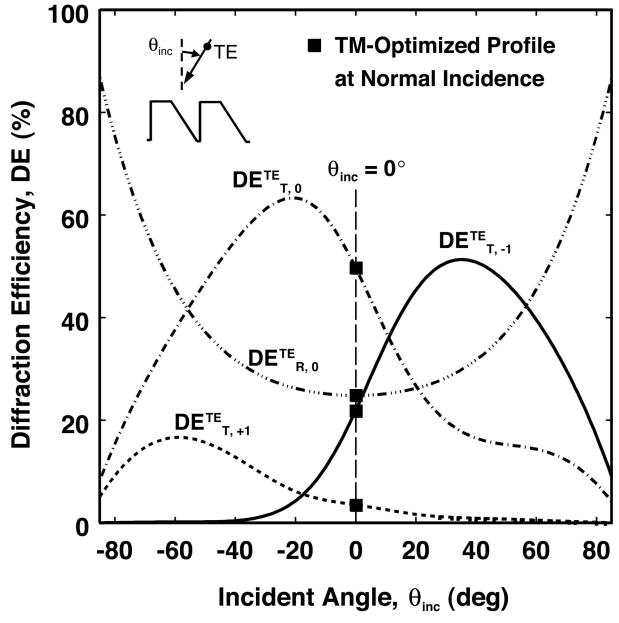

Fig. 9. Diffraction efficiencies as a function of incident angle θ_{inc} for the TM-optimized profile with a TE-polarized incidence.

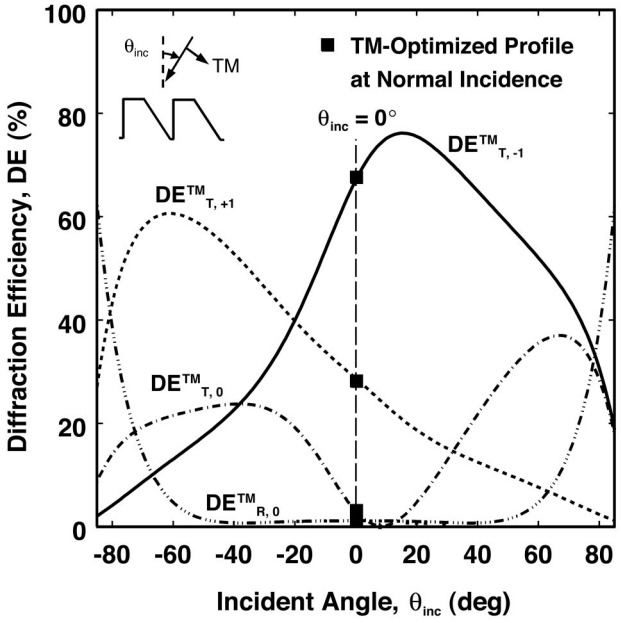

Fig. 10. Diffraction efficiencies as a function of incident angle θ_{inc} for the TM-optimized profile with a TM-polarized incidence.

$DE^{TM}_{T,-1} = 76.19\%$ at $\theta_{inc} = 15.41°$ for TE and TM polarizations, respectively. In addition, a comparison of Fig. 9 with Fig. 10 shows that the diffraction efficiency of $DE^{TM}_{T,+1}$ is much larger than that of $DE^{TE}_{T,+1}$, and the diffraction efficiency of $DE^{TM}_{R,0}$ is much smaller than that of $DE^{TE}_{R,0}$ because of the Brewster angle effect. In conclusion, the behavior of the angular sensitivities of the TM-optimized profile are consistent with those of the TE-optimized profiles for both TE and TM polarizations.

4. Summary

We have applied an optimization method based on a simulated annealing algorithm in conjunction with the rigorous coupled-wave analysis to determine the optimum profiles of right-angle-face anisotropically etched silicon surface-relief gratings for substrate-mode optical interconnects. TE, TM, and RL polarizations were investigated. The optimum diffraction efficiencies of the -1 forward-diffracted order $DE_{T,-1}$ of right-angle-face slanted Si SRGs are 37.29%, 67.10%, and 51.19% for TE-, TM-, and RL-polarization-optimized profiles, respectively. By comparison, V-groove Si SRGs have a maximum $DE_{T,-1}$ of 16.00%, 37.51%, and 24.30% for TE-, TM-, and RL-polarization-optimized profiles, respectively. In addition, we presented the sensitivities to the grating thickness, the slant angle, and the incident angle for both the TE-optimized profile and the TM-optimized profile of right-angle-face slanted SRGs. In general, $DE_{T,-1}$ increases (or decreases) as the slant angle decreases (or increases) from the angle of anisotropic etching $\phi = 54.736°$. Furthermore, as the incident angle increases (i.e., the incident plane wave moves toward the normal of slanted faces), $DE_{T,-1}$ increases. Finally, it should be noted that the present method

can be applied to obtain optimum designs of polymer SRGs to be fabricated with Si molds by use of nanoimprint lithography, a fabrication technique that could be applicable to inexpensive high-volume manufacturing.

This research was performed as part of the Interconnect Focus Center (IFC) research program supported by the Semiconductor Research Corporation (SRC), the Microelectronics Advanced Research Corporation (MARCO), and the Defense Advanced Research Projects Agency (DARPA).

References

1. J.-H. Yeh and R. K. Kostuk, "Substrate-mode holograms used in optical interconnects: design issues," Appl. Opt. **34,** 3152–3164 (1995).
2. J.-H. Yeh and R. K. Kostuk, "Free-space holographic optical interconnects for board-to-board and chip-to-chip interconnects," Opt. Lett. **21,** 1274–1276 (1996).
3. S.-D. Wu, T. K. Gaylord, E. N. Glytsis, and Y. -M. Wu, "Three-dimensional converging/diverging Gaussian beam diffraction by a volume grating," J. Opt. Soc. Am. A **22,** 1293–1303 (2005).
4. S.-D. Wu, T. K. Gaylord, E. N. Glytsis, and Y.-M. Wu, "Angular sensitivities of volume gratings for substrate-mode optical interconnects," Appl. Opt. **44,** 4447–4453 (2005).
5. S. M. Schultz, E. N. Glytsis, and T. K. Gaylord, "Design, fabrication, and performance of preferential-order volume grating waveguide couplers," Appl. Opt. **39,** 1223–1232 (2000).
6. R. A. Villalaz, E. N. Glytsis, and T. K. Gaylord, "Volume grating couplers: polarization and loss effects," Appl. Opt. **41,** 5223–5229 (2002).
7. S.-D. Wu and E. N. Glytsis, "Volume holographic grating couplers: rigorous analysis by use of the finite-difference frequency-domain method," Appl. Opt. **43,** 1009–1023 (2004).
8. S.-D. Wu, E. N. Glytsis, and T. K. Gaylord, "Optimization of finite-length input volume holographic grating couplers illuminated by finite-width incident beams," Appl. Opt. **44,** 4435–4446 (2005).
9. T. W. Ang, G. T. Reed, A. Vonsovici, A. G. R. Evans, P. R. Routley, and M. R. Josey, "Effects of grating heights on highly efficient unibound SOI waveguide grating couplers," IEEE Photon. Technol. Lett. **12,** 59–61 (2000).
10. R. Orobtchouk, A. Layadi, H. Gualous, D. Pascal, A. Koster, and S. Laval, "High-efficiency light coupling in a submicrometric silicon-on-insulator waveguide," Appl. Opt. **39,** 5773–5777 (2000).
11. D. Taillaert, P. Bienstman, and R. Baets, "Compact efficient broadband grating coupler for silicon-on-insulator waveguides," Opt. Lett. **29,** 2749–2751 (2004).
12. K. E. Bean, "Anisotropic etching of silicon," IEEE Trans. Electron Devices **25,** 1185–1193 (1978).
13. N. Rajkumar and J. N. McMullin, "V-groove gratings on silicon for infrared beam splitting," Appl. Opt. **34,** 2556–2559 (1995).
14. M. Auslender, D. Levy, and S. Hava, "One-dimensional antireflection gratings in (100) silicon: a numerical study," Appl. Opt. **37,** 369–373 (1998).
15. K. Sakaino and S. Adachi, "Study of Si(1 0 0) surfaces etched in TMAH solution," Sens. Actuators A **88,** 71–78 (2001).
16. S. Kirkpatrick, C. D. Gelatt, Jr., and M. P. Vecchi, "Optimization by simulated annealing," Science **220,** 671–680 (1983).
17. A. Corana, M. Marchesi, C. Martini, and S. Ridella, "Minimizing multimodal functions of continuous variables with the simulated annealing algorithm," ACM Trans. Math. Software **13,** 262–280 (1987).
18. T. K. Gaylord and M. G. Moharam, "Analysis and applications of optical diffraction by gratings," Proc. IEEE **73,** 894–937 (1985).